



Cite this: *RSC Adv.*, 2024, **14**, 2918

## Lithocholic acid derivatives as potent modulators of the nuclear receptor ROR $\gamma$ t $\dagger$

Somaya A. Abdel-Rahman,<sup>ab</sup> Simone Brogi,<sup>b</sup> and Moustafa T. Gabr,<sup>ab</sup>                                                                                                                                                                                                                                                                                  

transcription.<sup>39</sup> In addition, various synthetic inverse agonists, including T0901317 (1, Fig. 1),<sup>40</sup> target the same orthosteric ligand binding pocket in ROR $\gamma$ t. The identification of a novel allosteric binding site within the ROR $\gamma$ t LBD by potent ROR $\gamma$ t inverse agonists MRL-871 (2, Fig. 1)<sup>41</sup> and subsequently 3 (Fig. 1)<sup>42</sup> is based on the ability of these ligands to engage directly with the activation function loop situated between H11 and H12 (AF-2 domain), inducing an unconventional conformation in H12. This altered conformation effectively hinders the recruitment of coactivators. Notably, reports of ligands unequivocally directed towards the allosteric pocket of ROR $\gamma$ t are confined to compounds characterized by closely related chemotypes featuring indazole or imidazopyridine core.<sup>43</sup>

Numerous microbial metabolites serve as signaling molecules within the immune system and play a pivotal role in regulating immune homeostasis.<sup>44</sup> In this context, secondary bile acids have been identified as ligands for nuclear hormone receptors that modulate the differentiation of Th17 cells.<sup>45,46</sup> Specifically, 3-oxo-lithocholic acid (3-oxoLCA, 4, Fig. 1) and isolithocholic acid (isoLCA, 5, Fig. 1) have demonstrated an inhibitory effect on Th17 cell differentiation, which is significant in the context of autoimmune disorders.<sup>45,46</sup> Importantly, structural analogs of lithocholic acid have proven ineffective in mimicking the impact observed with 3-oxoLCA and isoLCA on Th17 cells.<sup>45,46</sup> While these findings have shed light on the role of bile acids in Th17 cell differentiation, questions persist, particularly regarding the underlying mechanisms responsible for the differential effects of structurally distinct bile acids on Th17 cell modulation.

Given the growing recognition of how immunomodulatory bile acid metabolites influence inflammatory conditions in humans, a more profound understanding of the structural characteristics that govern their immunomodulatory impact could pave the way for the development of therapeutic treatments targeting autoimmune and inflammatory diseases. Recent research has uncovered the ability of gut microbes in humans to conjugate bile acids with phenylalanine and tyrosine.<sup>47</sup> Building upon this discovery, we proposed a hypothesis suggesting that these bile acids, modified by gut microbes, belong to a larger group of compounds known as bile acid

amides, which include a wide range of structurally diverse biogenic amines. Thus, we hypothesized that the conjugation of bile acids to structurally diverse scaffolds would result in compounds with improved binding profiles to the corresponding targets of the parent bile acids. Herein, we introduce the potential of the 3-oxoLCA scaffold as a ROR $\gamma$ t ligand by evaluating a small library of compounds based on the conjugation of 3-oxoLCA to a variety of structurally diverse amines. We synthesized a series of 3-oxoLCA derivatives and their corresponding lithocholic acid (LCA) analogs as control compounds and evaluated the compounds as ROR $\gamma$ t ligands.

## Results and discussion

Initially, we conjugated the 3-oxoLCA and LCA cores to structurally diverse amines based on amide coupling chemistry (Scheme 1) using hexafluorophosphate benzotriazole tetramethyl uranium (HBTU) and triethylamine (TEA) in dimethylformamide (DMF). We selected these structurally diverse amines to introduce both hydrophobic and hydrogen bonding interactions into the proposed binding profiles of 3-oxoLCA and LCA to ROR $\gamma$ t. We confirmed the identity of the synthesized bile acid amides (**A2–A6** and **B2–B6**, Table 1) using nuclear magnetic resonance (NMR) and high-resolution mass spectrometry (HRMS). In addition, we determined the purity by high-performance liquid chromatography (HPLC) to be  $\geq 95\%$ .

Given that 3-oxoLCA (**A1**, Table 1) binds ROR $\gamma$ t at an equilibrium dissociation constant ( $K_D$ ) of  $\sim$ 1.1  $\mu$ M,<sup>45</sup> we analyzed the binding affinity of the synthesized bile acid amides (**A2–A6** and **B2–B6**) to ROR $\gamma$ t using microscale thermophoresis (MST). We performed the assay by labeling recombinant human ROR $\gamma$ t with the Monolith NT Protein Labeling Kit RED (NanoTemper Technologies). In our hands, 3-oxoLCA (**A1**) demonstrated a  $K_D$  value of  $\sim$ 1.08  $\pm$  0.09  $\mu$ M for ROR $\gamma$ t binding based on MST analysis (Table 1), which is in close agreement with the reported binding affinity.<sup>45</sup> Compounds **A2–A6**, based on the 3-oxoLCA scaffold, displayed submicromolar binding affinities to ROR $\gamma$ t according to MST analysis. Specifically, compound **A2** bearing a methoxy-substituted tryptamine moiety revealed the maximum enhancement in the ROR $\gamma$ t binding affinity in comparison to 3-oxoLCA (**A1**) with  $\sim$ 65-fold enhancement ( $K_D$  value of  $16.5 \pm 1.34$  nM, Fig. 2 and Table 1). Replacing the tryptamine scaffold in **A2** with a 2-benzhydryl moiety in **A3** resulted in a slight reduction in the ROR $\gamma$ t binding affinity, indicating the loss of potential hydrogen bonding interaction in **A2** with ROR $\gamma$ t ( $K_D = 16.5 \pm 1.34$  nM and  $57.2 \pm 3.01$  nM for **A2** and **A3**, respectively, Table 1). As illustrated in Table 1, incorporation of the biphenyl ethyl fragment into the 3-oxoLCA

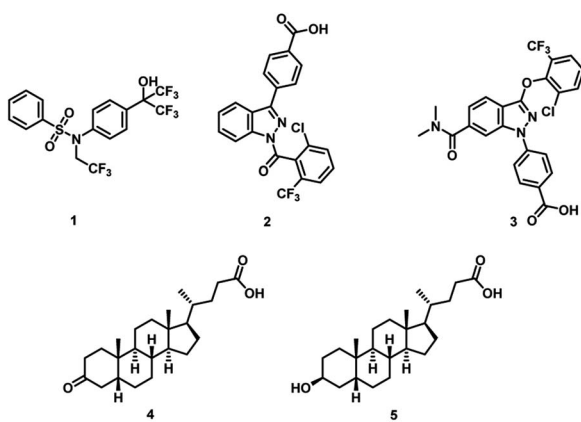
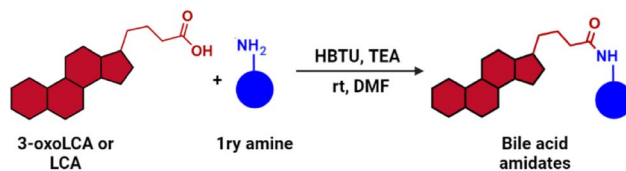
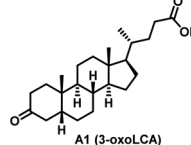
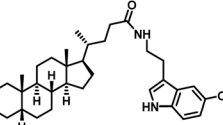
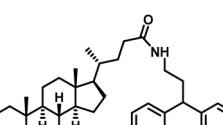
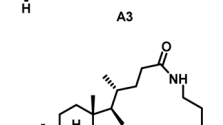
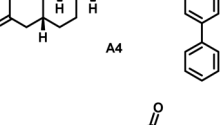
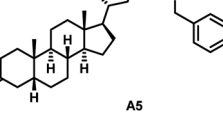
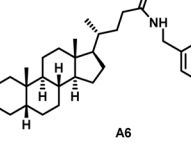
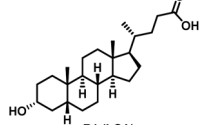
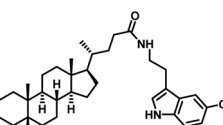


Fig. 1 Chemical structures of reported ROR $\gamma$ t modulators.

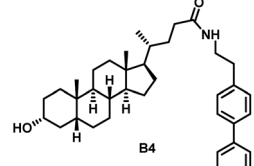
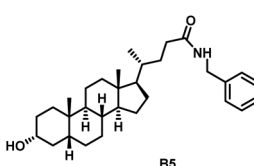
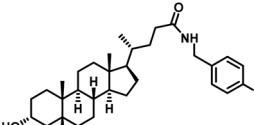


**Scheme 1** Synthesis of bile acid amides via amide coupling.

**Table 1** Chemical structures of the parent bile acids (A1 and B1) and the synthesized bile acid amides (A2–A6 and B2–B6) along with their binding affinity to ROR $\gamma$ t using MST

Compound	MST $K_D$ (nM) for ROR $\gamma$ t
	1083 $\pm$ 93.4
	16.5 $\pm$ 1.34
	57.2 $\pm$ 3.01
	87.4 $\pm$ 5.52
	724 $\pm$ 20.4
	618 $\pm$ 19.3
	28 534 $\pm$ 304
	9361 $\pm$ 131
	12 414 $\pm$ 267

**Table 1 (Contd.)**

Compound	MST $K_D$ (nM) for ROR $\gamma$ t
	15 789 $\pm$ 334
	27 103 $\pm$ 218
	24 868 $\pm$ 591

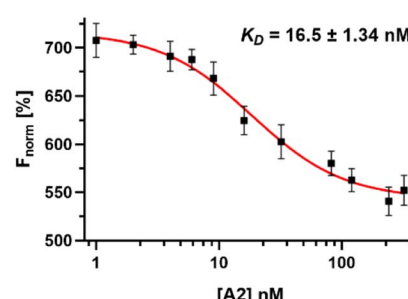


**Fig. 2** Dose–response curve of compound A2 binding to ROR $\gamma$ t LBD using MST. Error bars represent standard deviation ( $n = 3$ ).

scaffold in **A4** resulted in a remarkable enhancement in ROR $\gamma$ t binding affinity compared with benzyl substituents in **A5** and **A6**. This outcome indicates the significance of the elongated linker and the extended hydrophobic surface in **A4** compared with those in **A5** and **A6** in terms of maximizing the ROR $\gamma$ t binding affinity. Notably, we observed a similar trend regarding the outcome of the investigated moieties in modulating the ROR $\gamma$ t binding affinity of LCA (**B1**), as evident from the ROR $\gamma$ t binding affinities of **B2–B6** (Table 1). However, none of the synthesized LCA derivatives (**B2–B6**) possessed submicromolar ROR $\gamma$ t binding affinity according to MST analysis (Table 1). This outcome is in agreement with the reported superiority of 3-oxoLCA to LCA in ROR $\gamma$ t binding and modulating Th17-cell proliferation.<sup>45</sup> Thus, we conclude that further structural modifications of the 3-oxoLCA derivatives (**A2–A6**) rather than LCA derivatives (**B2–B6**) have the potential to result in the identification of novel ROR $\gamma$ t modulators with single-digit nanomolar or subnanomolar binding affinity.



Molecular docking studies were conducted to investigate the binding mode of the synthesized compounds and to explore the features responsible for the reduction in affinity of compounds **B1–B6** with respect to compounds **A1–A6** for the ROR $\gamma$ t LBD. These two series differ from the presence of a carbonyl function in compounds **A1–A6** in place of the hydroxyl function in compounds **B1–B6** series. This difference is responsible for a decrease in the affinity of the **B**-compound series compared with that of the **A**-compound series. For this purpose, we coupled the molecular docking studies with the evaluation of  $\Delta G_{\text{bind}}$ , as previously described by us,<sup>48,49</sup> because in this way, it is possible to capture the small structural differences that influenced the binding affinity. In general, the docking scores and the  $\Delta G_{\text{bind}}$  are significantly different between the two series, indicating that the presence of hydroxyl function (compounds **B1–B6**) is detrimental to the affinity of this series of compounds. In contrast, the presence of carbonyl function, as in compounds **A1–A6**, was well tolerated by the receptor, and the computational scores were favorable with respect to compounds **B1–B6** (Table 2). Notably, the docking scores and the  $\Delta G_{\text{bind}}$  of compounds **A1–A6** are comparable to those of the reference compound digoxin, which is a well-known antagonist of the ROR $\gamma$ t receptor.

In particular, as depicted in Fig. 3, compounds **A1–A6** showed relevant interactions with the ROR $\gamma$ t LBD. Starting from compound **A1** (Fig. 3A), the steroid-like core is located in the hydrophobic pocket composed of the following amino acids: Leu287, Leu324, Ala327, Val361, Phe377, and Phe388, whereas the carbonyl group established an H-bond with Arg367. The introduction of pendant substituents containing aromatic functions, as in compounds **A2–A6**, allowed the compounds to target further residents with respect to **A1**. This is reflected by a dramatic increase in affinity, as observed in biophysical screening and indicated by computational scores. In fact, compounds **A2–A6** were able to target, in addition to the previously mentioned residues, Trp317, Leu391, and His479 by H-bonds and/or  $\pi$ – $\pi$  stacking and hydrophobic interactions. The carbonyl function in compounds **A2–A6** preferably established an H-bond with the backbone of residue Leu287. The

**Table 2** Calculated parameters related to the molecular docking studies of A1–A6 and B1–B6 compounds

Compound	GlideScore (kcal mol <sup>-1</sup> )	$\Delta G_{\text{bind}}$ (kcal mol <sup>-1</sup> )
<b>A1</b>	-9.165	-88.91
<b>A2</b>	-10.711	-125.38
<b>A3</b>	-11.683	-121.47
<b>A4</b>	-10.807	-131.75
<b>A5</b>	-10.898	-114.26
<b>A6</b>	-10.942	-115.89
<b>B1</b>	-7.288	-79.24
<b>B2</b>	-9.107	-97.73
<b>B3</b>	-8.371	-93.22
<b>B4</b>	-9.386	-102.15
<b>B5</b>	-9.477	-91.83
<b>B6</b>	-10.088	-94.71
Digoxin	-12.278	-123.69

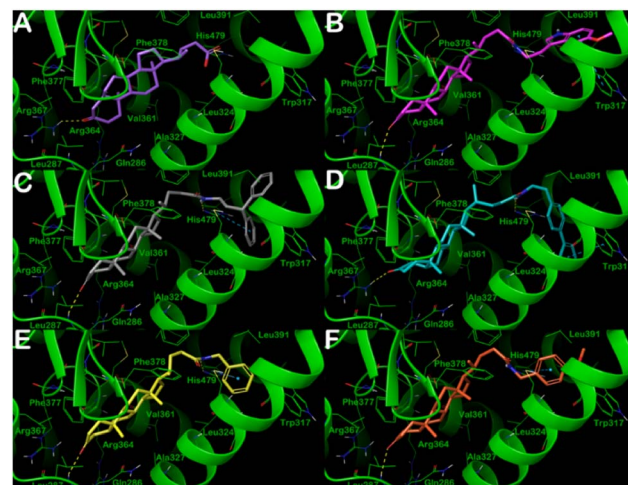


**Fig. 3** Putative binding mode of compounds A1–A6 (panels A–F, respectively) into ROR $\gamma$ t LBD (PDB ID: 3B0W). Key residues of the binding site are represented by lines and labeled. H-bonds and  $\pi$ – $\pi$  stacking interactions are illustrated as yellow and cyan dotted lines, respectively. Pictures were generated by Maestro (Maestro, Schrödinger LLC, release 2020-3).

increase in the number of contacts of compounds **A2–A6**, along with the calculation of the relative binding affinity, is in good agreement with the submicromolar affinity found for these compounds for the ROR $\gamma$ t receptor.

In contrast, the docking output for compounds **B1–B6** (Fig. 4) indicated that the introduction of the hydroxyl function is deleterious for their binding mode. In fact, none of the compounds could fruitfully bind to the binding site of the ROR $\gamma$ t receptor. We observed a dramatic decrease in the number and quality of contacts with respect to compounds **A1–**

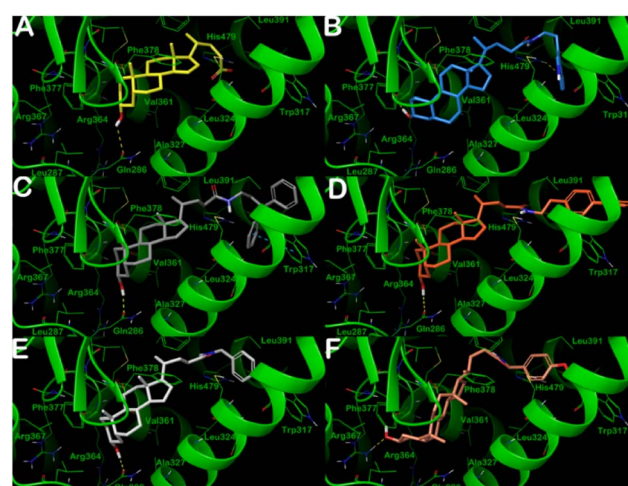


**Fig. 4** Putative binding mode of compounds B1–B6 (panels A–F, respectively) into ROR $\gamma$ t ligand binding domain (PDB ID: 3B0W). Key residues of the binding site are represented by lines and labeled. H-bonds and  $\pi$ – $\pi$  stacking interactions are illustrated as yellow and cyan dotted lines, respectively. Pictures were generated by Maestro (Maestro, Schrödinger LLC, release 2020-3).

**A6.** This is reflected in a significant decrease in the docking scores and the  $\Delta G_{\text{bind}}$ , indicating a decrease in affinity, as found by the MST binding analysis. In particular, the pendant substituents were no longer able to strongly target the residues Trp317 and His479, except for the biphenyl-containing compound **B3**, which established a  $\pi$ - $\pi$  stacking with Trp317. The hydroxyl function could not target Leu287 or Arg367 (with exclusion of **B6**), whereas it targeted the side chain of Gln286 by an H-bond. This indicated that compounds **B1–B6** could not penetrate deeply into the selected binding site. The significant reduction in the number of contacts along with unfavorable conformational energies, docking scores, and an increase of  $\Delta G_{\text{bind}}$  for the compounds **B1–B6** culminated in a drastic reduction in the affinity for ROR $\gamma$ t receptor in the high micro-molar range, highlighting that a small structural difference could have a significant effect on binding interactions.

In order to evaluate the *in vitro* ROR $\gamma$ t cellular binding of the synthesized compounds, we implemented the established GAL4-ROR $\gamma$  reporter assay based on proprietary human cells engineered to provide high-level expression of a hybrid human ROR $\gamma$ . The reporter cells incorporate cDNA encoding beetle luciferase, which catalyzes the oxidation of d-luciferin, resulting in photon emission. In the reporter assay, the N-terminal DNA-binding domain (DBD) of the native ROR $\gamma$  receptor has been replaced with the DBD of the yeast GAL4.<sup>50,51</sup> Ligands of ROR $\gamma$  (antagonists or inverse agonists) would reduce the affinity of GAL4-ROR $\gamma$  to the DNA site and minimize the luminescence signal. Initially, we screened **A1–A6** and **B1–B6** in the ROR $\gamma$  reporter assay at a single concentration of 1  $\mu$ M using ML-209 and digoxin as positive control compounds. As shown in Fig. 5A, the outcome of the ROR $\gamma$  reporter assay was in agreement with that of our ROR $\gamma$  binding analysis using MST with compounds **A1–A6**, revealing a superior reduction in luminescence of reporter cells to compounds **B1–B6**, indicating an efficient inhibition of the binding of GAL4-ROR $\gamma$  to the DNA site. Among **A1–A6** and **B1–B6**, compound **A2** demonstrated the most pronounced reduction in the luminescence signal in single-dose screening (Fig. 5A). Unlike compounds **A5** and **A6**, a potent decrease in the luminescence from the reporter cells was observed for **A3** and **A4** in single-dose screening (Fig. 5A). However, **B1–B6** failed to induce a significant decrease in luminescence of reporter cells in single-dose screening (Fig. 5A). Dose-dependent screening of the most potent compound from our study (**A2**) using the ROR $\gamma$  reporter assay revealed a half-maximal inhibitory concentration ( $IC_{50}$ ) of  $225 \pm 10.4$  nM (Fig. 5B). It is noteworthy to mention that the positive control (ML-209) possessed an  $IC_{50}$  value of  $127.9 \pm 18.3$  nM in the ROR $\gamma$  reporter assay (Fig. S1, ESI<sup>†</sup>).

We further evaluated the cellular activity of the compounds by assessing the reduction of IL-17A mRNA expression levels using quantitative reverse transcriptase PCR (RT-PCR) in EL4 cells (a murine lymphoblast cell line with validated ROR $\gamma$ t expression). Treatment of EL4 cells with **A1** (3-oxoLCA), **A2**, and **A3** at 10  $\mu$ M tested concentration for 24 h revealed a potent reduction in IL-17A expression by both **A2** and **A3** (Fig. 6). In contrast, 3-oxoLCA (**A1**) induced a minimal change in IL-17A expression in EL4 cells (Fig. 6). These findings indicate the

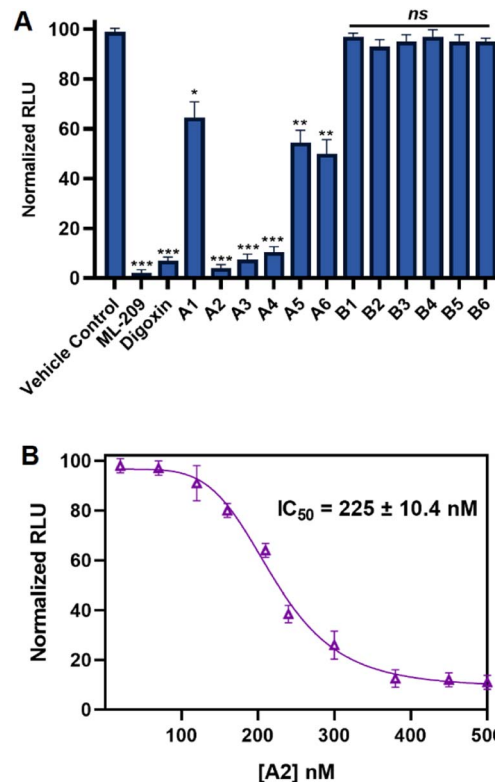


Fig. 5 (A) Single-dose screening of **A1–A6** and **B1–B6** at 1  $\mu$ M ( $n = 3$ ) in the ROR $\gamma$ t reporter luciferase assay using ML-209 and digoxin (1  $\mu$ M,  $n = 3$ ) as positive controls. RLU stands for relative luminescence units from the reporter assay. \* $p < 0.05$ , \*\* $p < 0.01$ , \*\*\* $p < 0.001$ , and ns denotes non-significant in comparison to vehicle control. (B) Dose-response curve of compound **A2** in the ROR $\gamma$ t reporter luciferase assay. Error bars represent standard deviation ( $n = 3$ ).

potential of the synthesized bile acid amides as ROR $\gamma$  modulators compared with the parent bile acids. Notably, bile acid derivatives exhibit high cross-reactivity toward ROR $\alpha$  and ROR $\gamma$ t with high affinities.<sup>52</sup> Interestingly, **A2** revealed >100-fold

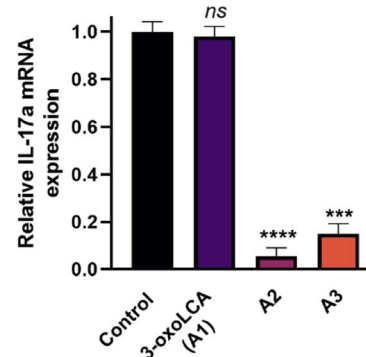


Fig. 6 IL-17A mRNA expression in EL4 cells incubated with a single dose (10  $\mu$ M,  $n = 3$ ) of 3-oxoLCA (**A1**), **A2**, **A3**, or vehicle control (DMSO). The level of IL-17A expression was normalized to that of GAPDH expression. \*\*\* $p < 0.001$ , \*\*\*\* $p < 0.0001$ , and ns denotes non-significant in comparison to vehicle control. Error bars represent standard deviation ( $n = 3$ ).



Table 3 Key physicochemical properties for the top compounds from this study

Compound	Solubility <sup>a</sup> (μM)	log P <sup>b</sup>	HSA binding <sup>c</sup>	Chemical stability <sup>d</sup> (% remaining)	Plasma stability <sup>e</sup> (% remaining)
<b>A2</b>	72	2.93	81	98.1	95.7
<b>A3</b>	12	3.87	94	99.3	97.4
<b>A4</b>	9	3.96	96	99.1	96.9

<sup>a</sup> Water solubility of the compounds as protonated species. <sup>b</sup> 1-Octanol-water partition coefficient. <sup>c</sup> Albumin binding. <sup>d</sup> Stability in simulated intestinal fluid (2 h incubation). <sup>e</sup> Stability in human plasma (2 h incubation).

selectivity for binding ROR $\gamma$ t over ROR $\alpha$  according to MST binding analysis (Fig. S2, ESI $\dagger$ ). On the other hand, 3-oxoLCA (**A1**) possessed  $\sim$ 2-fold selectivity for ROR $\gamma$ t binding over ROR $\alpha$  (Fig. S3, ESI $\dagger$ ). The remarkable enhancement in selective ROR $\gamma$ t binding for our new class of bile acid amides highlights the significance of our work.

In order to assess the potential of the developed compounds for preclinical evaluation, we assessed the key physicochemical properties and stability of the three best performing compounds from this study (**A2**, **A3**, and **A4**). As shown in Table 3, compound **A2** exhibited remarkable enhancement in aqueous solubility in the protonated state compared with **A3** and **A4**. The three compounds studied (**A2**, **A3**, and **A4**) possessed favorable profiles as potential drug candidates in terms of lipophilicity, human serum albumin (HSA) binding, stability in simulated intestinal fluid, and stability upon incubation with human plasma (Table 3). This likely indicates that further optimization of this class of 3-oxoLCA amides can result in candidate molecules with desirable *in vivo* efficacy in models of autoimmune and inflammatory diseases.

## Conclusions

In summary, we have introduced 3-oxoLCA amides as potent modulators of ROR $\gamma$ t. In comparison to 3-oxoLCA (**A1**), the top compounds from this study (**A2** and **A3**) possessed nanomolar binding affinity to ROR $\gamma$ t in biophysical screening, exhibited functional activity in the ROR $\gamma$ t reporter assay at sub-micromolar concentrations, and inhibited the IL-17A mRNA expression in EL4 cells. We conducted a computational study to rationalize the superiority of **A1–A6** compounds to **B1–B6** compounds as ROR $\gamma$ t ligands. Moreover, we verified the desirable physicochemical properties and stability of the most potent ROR $\gamma$ t modulators. We anticipate that this study will trigger future research aiming to realize the potential of 3-oxoLCA amides as ROR $\gamma$ t modulators in animal models of autoimmune diseases.

## Experimental

### General

All commercially available starting materials, reagents, and solvents were used as supplied unless otherwise stated. The reported yields are isolated yields. Proton ( $^1\text{H}$ ) and carbon ( $^{13}\text{C}$ ) NMR were collected on Bruker NMR spectrometers at 400 MHz for  $^1\text{H}$  and 100 MHz for  $^{13}\text{C}$ . Chemical shifts ( $\delta$ ) are reported in parts-per million (ppm) relative to the residual undeuterated

solvent. High resolution mass spectra were obtained in the positive ion mode using electrospray ionization (ESI) on a double-focusing magnetic sector mass spectrometer.

### General method for the synthesis of **A2–A6** and **B2–B6**

2 mmol (1 eq.) 3-oxoLCA (**A1**) or LCA (**B1**) was added in a round bottom flask in  $\text{N}_2$  atmosphere, and 5 mL of DMF. The corresponding primary amine (1.1 eq.), HBTU (1.1 eq.) and triethyl amine (TEA, 1.2 eq.) were then added. The reaction mixture was allowed to stir overnight at room temperature. Subsequently, the reaction mixture was diluted with ethyl acetate (75 mL), washed with 5% HCl, 10%  $\text{Na}_2\text{CO}_3$  and brine, and dried over anhydrous  $\text{Na}_2\text{SO}_4$ . The organic layer was concentrated under reduced pressure to give the crude product, which was further purified by flash column chromatography using a gradient of hexane and ethyl acetate as the solvent system.

**A2.** (4R)-4-((8R,9S,10S,13R,14S,17R)-10,13-Dimethyl-3-oxohexadecahydro-1*H*-cyclopenta[*a*]phenanthren-17-yl)-N-(2-(methoxy-1*H*-indol-2-yl)ethyl)pentanamide.  $^1\text{H}$  NMR (DMSO-d<sub>6</sub>,  $\delta$  ppm): 0.68 (s, 3H,  $\text{CH}_3$ ), 0.91 (d, 3H,  $\text{CH}_3$ ), 1.03 (s, 3H,  $\text{CH}_3$ ), 1.06–1.62 (m, 18H,  $\text{CH}$ ,  $\text{CH}_2$ ), 1.71–2.38 (m, 12H,  $\text{CH}$ ,  $\text{CH}_2$ ), 3.61 (q, 2H,  $\text{CH}_2$ ), 3.88 (s, 3H,  $\text{CH}_3$ ), 5.56 (t, 1H, NH), 6.9 (d, 1H, Ar-H), 7.03–7.06 (m, 2H, Ar-H), 7.30 (s, 1H, NH).  $^{13}\text{C}$  NMR (DMSO-d<sub>6</sub>,  $\delta$  ppm): 12.33, 18.81, 21.24, 22.70, 24.27, 25.78, 26.70, 28.19, 31.17, 31.24, 32.07, 32.94, 34.91, 35.41, 35.54, 36.26, 36.93, 37.18, 40.55, 42.33, 42.75, 44.07, 55.79, 56.11, 100.59, 111.42, 112.45, 123.68, 128.03, 131.84, 153.42, 162.80, 172.88, 212.33. HRMS (ESI): calculated for  $\text{C}_{35}\text{H}_{50}\text{N}_2\text{O}_3$  ( $\text{M} + \text{H}$ )<sup>+</sup>, 547.3899; found, 547.3895.

**A3.** (4R)-4-((8R,9S,10S,13R,14S,17R)-10,13-Dimethyl-3-oxohexadecahydro-1*H*-cyclopenta[*a*]phenanthren-17-yl)-N-(3,3-diphenylpropyl)pentanamide.  $^1\text{H}$  NMR ( $\text{CDCl}_3$ ,  $\delta$  ppm): 0.70 (s, 3H,  $\text{CH}_3$ ), 0.96 (d, 3H,  $\text{CH}_3$ ), 1.03 (s, 3H,  $\text{CH}_3$ ), 1.09–1.46 (m, 27H,  $\text{CH}$ ,  $\text{CH}_2$ ), 1.80–2.45 (m, 12H,  $\text{CH}$ ,  $\text{CH}_2$ ), 7.19–7.32 (m, 10H, Ar-H).  $^{13}\text{C}$  NMR (acetone-d<sub>6</sub>,  $\delta$  ppm): 11.68, 13.69, 18.11, 21.09, 22.18, 24.04, 25.65, 26.58, 28.05, 31.91, 32.85, 34.74, 35.34, 35.42, 36.75, 36.90, 37.79, 40.01, 40.26, 41.95, 42.63, 44.24, 48.89, 56.21, 59.69, 126.11, 127.81, 128.41, 145.05, 172.65, 210.57. HRMS (ESI): calculated for  $\text{C}_{39}\text{H}_{53}\text{NO}_2$  ( $\text{M} + \text{H}$ )<sup>+</sup>, 568.4149; found, 568.4143.

**A4.** (4R)-N-(2-([1,1'-Biphenyl]-4-yl)ethyl)-4-((8R,9S,10S,13R,14S,17R)-10,13-dimethyl-3-oxohexadecahydro-1*H*-cyclopenta[*a*]phenanthren-17-yl)pentanamide.  $^1\text{H}$  NMR (DMSO-d<sub>6</sub>,  $\delta$  ppm): 0.64 (s, 3H,  $\text{CH}_3$ ), 0.92–0.93 (m, 6H,  $3\text{CH}_2$ ), 1.01–1.35 (m, 10H,  $5\text{CH}_2$ ), 1.54–1.86 (m, 13H,  $5\text{CH}_2$ ,  $\text{CH}_3$ ), 1.95–1.97 (m, 2H,  $\text{CH}_2$ ), 2.19 (s, 3H,  $\text{CH}_3$ ), 2.88–2.90 (m, 2H,  $\text{CH}_2$ ), 3.55–3.59 (m, 1H,  $\text{CH}$ ), 5.51 (s, 1H, OH), 7.28–7.30 (t,



2H, Ar-H), 7.35–7.38 (t, 2H, Ar-H), 7.44–7.47 (m, 4H, Ar-H), 7.56–7.61 (m, 1H, Ar-H), 8.03 (s, 1H, NH).

<sup>13</sup>C NMR (DMSO-d<sub>6</sub>, δ ppm): 12.32, 18.76, 21.22, 22.68, 22.70, 24.24, 25.74, 26.69, 28.17, 31.17, 32.07, 32.90, 34.91, 35.35, 35.52, 36.92, 37.18, 42.33, 42.73, 43.91, 56.08, 56.16, 126.94, 127.01, 127.66, 129.73, 129.74, 138.41, 139.34, 140.52, 172.94, 212.33. HRMS (ESI): calculated for C<sub>38</sub>H<sub>51</sub>NO<sub>2</sub> (M + H)<sup>+</sup>, 554.3993; found, 554.3980.

**A5.** (4*R*)-*N*-Benzyl-4-((8*R*,9*S*,10*S*,13*R*,14*S*,17*R*)-10,13-dimethyl-3-oxohexadecahydro-1*H*-cyclopenta[*a*]phenanthren-17-yl)pentanamide. <sup>1</sup>H NMR (CDCl<sub>3</sub>, δ ppm): 0.65 (s, 3H, CH<sub>3</sub>), 0.95 (d, 3H, CH<sub>3</sub>), 1.03 (s, 3H, CH<sub>3</sub>), 1.07–1.66 (m, 22H, CH, CH<sub>2</sub>), 1.81–2.53 (m, 8H, CH<sub>2</sub>), 7.30–7.36 (m, 5H, Ar-H), 7.58 (s, 1H, NH). <sup>13</sup>C NMR (DMSO-d<sub>6</sub>, δ ppm): 12.29, 18.73, 21.24, 22.68, 25.76, 26.69, 28.21, 31.13, 32.08, 32.81, 34.89, 35.35, 35.53, 42.45, 42.75, 56.12, 127.12, 127.61, 128.66, 140.19, 173.07, 212.27. HRMS (ESI): calculated for C<sub>31</sub>H<sub>45</sub>NO<sub>2</sub> (M + H)<sup>+</sup>, 464.3523; found, 464.3527.

**A6.** (4*R*)-4-((8*R*,9*S*,10*S*,13*R*,14*S*,17*R*)-10,13-Dimethyl-3-oxohexadecahydro-1*H*-cyclopenta[*a*]phenanthren-17-yl)-*N*-(4-methoxybenzyl)pentanamide. <sup>1</sup>H NMR (CDCl<sub>3</sub>, δ ppm): 0.68 (s, 3H, CH<sub>3</sub>), 0.92 (d, 3H, CH<sub>3</sub>), 1.02 (s, 3H, CH<sub>3</sub>), 1.08–1.62 (m, 17H, CH, CH<sub>2</sub>), 1.80–2.14 (m, 11H, CH, CH<sub>2</sub>), 2.25–2.37 (m, 2H, CH<sub>2</sub>), 3.80 (s, 3H, CH<sub>3</sub>), 4.37 (d, 2H, CH<sub>2</sub>), 5.82 (s, 1H, NH), 6.86 (d, 2H, Ar-H), 7.21 (d, 2H, Ar-H). <sup>13</sup>C NMR (DMSO, δ ppm): 12.31, 18.78, 21.23, 22.70, 24.27, 25.75, 26.70, 28.20, 31.17, 32.07, 32.80, 34.92, 35.35, 35.54, 36.93, 37.18, 38.72, 41.87, 42.33, 42.76, 44.06, 55.52, 56.10, 114.10, 128.91, 132.20, 158.48, 172.86, 212.45. HRMS (ESI): calculated for C<sub>32</sub>H<sub>47</sub>NO<sub>3</sub> (M + H)<sup>+</sup>, 494.3629; found, 494.3627.

**B2.** (4*R*)-4-((3*R*,8*R*,9*S*,10*S*,13*R*,14*S*,17*R*)-3-Hydroxy-10,13-dimethylhexadecahydro-1*H*-cyclopenta[*a*]phenanthren-17-yl)-*N*-(2-(5-methoxy-1*H*-indol-2-yl)ethyl)pentanamide. <sup>1</sup>H NMR (DMSO-d<sub>6</sub>, δ ppm): 0.61 (s, 3H, CH<sub>3</sub>), 0.94–2.13 (m, 35H, CH, CH<sub>2</sub>), 3.77 (s, 3H, CH<sub>3</sub>), 4.46 (d, 1H, Ar-H), 6.72 (d, 1H, Ar-H), 7.01 (d, 1H, Ar-H), 7.09 (d, 1H, Ar-H), 7.23 (d, 1H, Ar-H), 7.87 (t, 1H, NH), 7.97 (s, 1H, NH), 10.63 (s, 1H, OH). HRMS (ESI): calculated for C<sub>35</sub>H<sub>52</sub>N<sub>2</sub>O<sub>3</sub> (M + H)<sup>+</sup>, 549.4056; found, 549.4059.

**B3.** (4*R*)-*N*-(3,3-Diphenylpropyl)-4-((3*R*,8*R*,9*S*,10*S*,13*R*,14*S*,17*R*)-3-hydroxy-10,13-dimethylhexadecahydro-1*H*-cyclopenta[*a*]phenanthren-17-yl)pentanamide. <sup>1</sup>H NMR (CDCl<sub>3</sub>, δ ppm): 0.65 (s, 3H, CH<sub>3</sub>), 0.66 (s, 3H, CH<sub>3</sub>), 0.93 (d, 3H, CH<sub>3</sub>), 1.26–1.28 (m, 4H, CH, CH<sub>2</sub>), 1.53–1.97 (m, 18H, CH, CH<sub>2</sub>), 2.14–2.34 (m, 4H, CH, CH<sub>2</sub>), 2.82–2.84 (m, 2H, CH<sub>2</sub>), 3.26–3.27 (m, 2H, CH<sub>2</sub>), 3.64–3.78 (m, 1H, CH), 3.97–4.00 (m, 1H, CH), 5.46 (s, 1H, NH), 7.22–7.32 (m, 10H, Ar-H). <sup>13</sup>C NMR (CDCl<sub>3</sub>, δ ppm): 12.36, 18.77, 20.87, 23.75, 24.32, 26.64, 27.36, 28.19, 29.79, 30.85, 31.98, 32.82, 34.68, 35.35, 35.61, 35.85, 36.77, 40.08, 40.24, 40.41, 40.64, 40.69, 41.99, 42.74, 56.04, 56.57, 70.33, 124.63, 125.56, 127.37, 142.17, 173.09. HRMS (ESI): calculated for C<sub>39</sub>H<sub>55</sub>NO<sub>2</sub> (M + H)<sup>+</sup>, 570.4306; found, 570.4295.

**B4.** (4*R*)-*N*-(2-[[1,1'-Biphenyl]-4-yl]ethyl)-4-((3*R*,8*R*,9*S*,10*S*,13*R*,14*S*,17*R*)-3-hydroxy-10,13-dimethylhexadecahydro-1*H*-cyclopenta[*a*]phenanthren-17-yl)pentanamide. <sup>1</sup>H NMR (DMSO-d<sub>6</sub>, δ ppm): 0.64 (s, 3H, CH<sub>3</sub>), 0.92 (d, 3H, CH<sub>3</sub>), 0.93 (s, 3H, CH<sub>3</sub>), 0.98–2.11 (m, 30H, CH, CH<sub>2</sub>), 2.23–2.30 (m, 1H, CH), 2.89 (t, 2H, CH<sub>2</sub>), 3.57–3.68 (m, 3H, CH, CH<sub>2</sub>), 5.63 (s, 1H, OH), 7.30 (s, 1H, NH), 7.35–7.38 (m, 1H, Ar-H), 7.46 (t, 2H, Ar-H), 7.57–7.61 (m, 4H, Ar-H). <sup>13</sup>C NMR (CDCl<sub>3</sub>, δ ppm): 12.07, 18.37, 20.82, 23.38, 24.20,

26.41, 27.20, 28.25, 30.55, 34.57, 35.34, 35.84, 36.50, 40.18, 40.42, 40.49, 42.09, 42.73, 56.01, 56.48, 71.86, 126.99, 127.34, 128.79, 129.24, 138.06, 139.47, 140.80, 162.55, 173.62. HRMS (ESI): calculated for C<sub>38</sub>H<sub>52</sub>NO<sub>2</sub> (M + H)<sup>+</sup>, 556.4149; found, 556.4149.

**B5.** (4*R*)-*N*-Benzyl-4-((3*R*,8*R*,9*S*,10*S*,13*R*,14*S*,17*R*)-3-hydroxy-10,13-dimethylhexadecahydro-1*H*-cyclopenta[*a*]phenanthren-17-yl)pentanamide. <sup>1</sup>H NMR (DMSO-d<sub>6</sub>, δ ppm): 0.62 (s, 3H, CH<sub>3</sub>), 0.90 (d, 3H, CH<sub>3</sub>), 0.91 (s, 3H, CH<sub>3</sub>), 1.02–1.37 (m, 12H, CH, CH<sub>2</sub>), 1.50–2.18 (m, 9H, CH, CH<sub>2</sub>), 4.26 (d, 2H, CH<sub>2</sub>), 4.45–4.47 (m, 1H, CH), 7.23–7.33 (m, 5H, Ar-H), 8.31 (t, 1H, NH). HRMS (ESI): calculated for C<sub>31</sub>H<sub>47</sub>NO<sub>2</sub> (M + H)<sup>+</sup>, 465.3680; found, 464.3534.

**B6.** (4*R*)-4-((3*R*,8*R*,9*S*,10*S*,13*R*,14*S*,17*R*)-3-Hydroxy-10,13-dimethylhexadecahydro-1*H*-cyclopenta[*a*]phenanthren-17-yl)-*N*-(4-methoxybenzyl)pentanamide. <sup>1</sup>H NMR (DMSO-d<sub>6</sub>, δ ppm): 0.61 (s, 3H, CH<sub>3</sub>), 0.89 (s, 3H, CH<sub>3</sub>), 0.90 (d, 3H, CH<sub>3</sub>), 1.03–1.37 (m, 18H, CH, CH<sub>2</sub>), 1.50–2.07 (m, 10H, CH, CH<sub>2</sub>), 3.36–3.41 (m, 1H, CH), 3.74 (s, 3H, CH<sub>3</sub>), 4.18 (d, 2H, CH<sub>2</sub>), 4.45 (d, 1H, OH), 6.88 (d, 2H, Ar-H), 7.17 (d, 2H, Ar-H), 8.22 (t, 1H, NH). <sup>13</sup>C NMR (DMSO-d<sub>6</sub>, δ ppm): 12.33, 18.75, 20.87, 23.75, 24.32, 26.64, 27.36, 28.21, 30.85, 31.24, 32.08, 32.82, 34.68, 35.36, 35.61, 35.85, 36.26, 36.76, 41.87, 41.99, 42.43, 42.73, 55.51, 55.67, 56.05, 56.57, 70.34, 114.09, 128.97, 130.86, 132.20, 158.60, 162.76, 172.89. HRMS (ESI): calculated for C<sub>32</sub>H<sub>49</sub>NO<sub>3</sub> (M + H)<sup>+</sup>, 496.3785; found, 496.3780.

### MST assay

For MST screening, we used Monolith NT.115 instrument from Nanotemper to assess the compounds/ROR $\gamma$ t interaction. We procured recombinant human ROR $\gamma$ t from WuXi and labeled it with Protein Labeling Kit RED-NHS 2nd Generation from Nanotemper (Cat #MO-L011). ROR $\gamma$ t was produced by recombinant microbial expression from *E. coli* cells (BL21-CodonPlus (DE3)-RIL Competent Cells, Cat #230245 from AGILENT). We dissolved ROR $\gamma$ t in PBS buffer (pH 7.4) with 0.1% bovine serum albumin (BSA) and 0.05% Tween 20. We kept the concentration of the fluorescently labeled ROR $\gamma$ t constant at 25 nM. We added a volume of 5  $\mu$ L of the corresponding samples in MST capillaries with a final DMSO concentration of 2%. Subsequently, we incubated the samples within the capillaries for 20 min at room temperature prior to the measurements. We detected changes in thermophoretic properties as a change in fluorescence intensity upon incubation of various concentrations of the tested compounds with fluorescently labeled ROR $\gamma$ t. We plotted the thermophoresis signal against the compound concentration to obtain a dose-response curves, from which  $K_D$  values can be deduced. MST data are represented as normalized change in fluorescence ( $F_{norm}$ ) upon ligand binding.  $F_{norm}$  is the ratio of the fluorescence measured before and during thermophoresis.

### Computational details

**Protein and ligand preparation.** Compound structures were built in Maestro Drug Discovery Suite (Maestro release 2020-3, Schrödinger, LLC, New York, NY, 2020) employing the available drawing tools, specifying the correct stereochemistry for each compound. The MacroModel application (MacroModel release



2020, Schrödinger, LLC, New York, NY, 2020) with the OPLS-2005 force field was used for energy minimization.<sup>53</sup> To simulate the solvent effect, the GBSA model was used with “no cutoff” for nonbonded interactions. The PRCG method (5000 maximum iterations and threshold for gradient convergence = 0.001) was utilized to minimize the potential energy. LigPrep software (LigPrep release 2020, Schrödinger, LLC, New York, NY, 2020) was used to treat the resulting compounds to provide the most probable ionization state at physiological pH (7.4 ± 0.2). The experimental structure of the ROR $\gamma$  ligand binding domain was downloaded from the Protein Data Bank (PDB ID: 3B0W);<sup>54</sup> crystal structure of ROR $\gamma$  LBD in complex with digoxin and imported into Maestro. Next, to refine and minimize the structure, we applied the Protein Preparation Wizard protocol available in Maestro as previously described.<sup>55,56</sup> We selected the mentioned PDB file because the crystallized ligand is the drug digoxin that is similar to our series of compounds sharing a steroid-like scaffold, and it is an antagonist of the ROR $\gamma$  receptor as our newly developed compounds presented in this work.

**Molecular docking.** Molecular docking studies were conducted in Maestro using Glide software (Glide release 2020, Schrödinger, LLC, New York, NY, 2020) with SP scoring function.<sup>57</sup> The energy grid for docking was prepared using the default value of the protein atom-scaling factor (1.0 Å), with a cubic box centered on the crystallized ligand. The docked poses considered for the post-docking minimization step were 1000. The selected docking protocol was able to correctly accommodate the crystallized ligand digoxin, as found during the redocking procedure for validating the docking protocol. To improve the quality of the investigation, we also calculated the relative ligand-binding energies from the complexes derived by molecular docking studies using the Prime/MM-GBSA method (Prime release 2020, Schrödinger, LLC, New York, NY, USA, 2020) as previously described.<sup>48</sup> This technique computes the variation between the free and complex states of both the ligand and enzyme after energy minimization.

### ROR $\gamma$ reporter assay

We procured the ROR $\gamma$  reporter assay kit (Cat#IB04001) from INDIGO Biosciences (State College, PA, USA) to assess the inhibitory activity of the compounds in comparison to DMSO vehicle and control compounds. We performed the assay following the manufacturer's recommended protocol. Briefly, we dispensed 200 μL of reporter cells per well in 96-well plates and pre-incubated the cells for 6 h. We prepared samples of the tested compounds ( $n = 3$ ) at 1 μM in single-dose screening or at multiple concentrations in dose-dependent screening in treatment media in the presence of 0.4% DMSO. After discarding the culture media post pre-incubation, 200 μL per well of the prepared treatment media was added. Following a 24 h incubation, treatment media were removed, and luciferase detection reagents were introduced to each well. The intensity of light emission, measured in relative light units (RLUs), from each well was quantified using a plate-reading luminometer. This assay was performed in a single run ( $n = 3$ ). The statistical

significance levels were denoted as follows: \* $p < 0.05$ , \*\* $p < 0.01$ , \*\*\* $p < 0.001$ , and ‘ns’ indicating non-significance in comparison to the vehicle control.

### Quantitative IL-17A mRNA RT-PCR assay

This assay was conducted using EL4 cells (Sigma-Aldrich), cultured in DMEM (Gibco) with 10% FBS. After seeding the cells onto a 12-well plate, they were incubated in the presence of 10 μM compound ( $n = 3$ , prepared from DMSO stock solutions) or DMSO (vehicle control) for 24 h. Subsequently, the cells were activated with phorbol 12-myristate 13-acetate (PMA, 50 ng mL<sup>-1</sup>; Sigma-Aldrich) and ionomycin (1 μg mL<sup>-1</sup>; Sigma-Aldrich) for 5 h. Following activation, the cells were collected, and RNA was isolated using a RNeasy Mini Kit (Qiagen). Reverse transcription was performed using the iScript Advanced cDNA Synthesis Kit (Bio-Rad). Quantitative RT-PCR was carried out to assess mRNA levels of mouse IL-17A ( $n = 3$ ) utilizing SYBR green technology (Bio-Rad) on a CFX Real-Time System (Bio-Rad). Normalization of IL-17A mRNA expression to Gapdh expression was performed, and the relative gene expression was calculated using the 2<sup>-ΔΔCt</sup> (Livak) method with the DMSO control as the calibrator. This assay was performed in a single run ( $n = 3$ ). The statistical significance levels were denoted as follows: \*\*\* $p < 0.001$ , \*\*\*\* $p < 0.0001$ , and ‘ns’ indicating non-significance in comparison to the vehicle control.

### Water solubility

The tested compounds were suspended in 100 mL of 0.1 M HCl (pH 1.00) and the saturated solutions were transferred to a thermostat-equipped water bath (25 °C). Following the incubation time (48 h), we filtered the solutions and determined the concentration of the compounds by HPLC-ES-MS/MS.

### Lipophilicity ( $\log P$ )

We evaluated the 1-octanol/water partition coefficient using the conventional shake-flask method. We performed the experiment at 1 mM solution of the tested compound buffered at pH 7.4. We measured the concentration of the tested compound in the water phase before and after partitioning in 1-octanol using HPLC-ES-MS/MS.

### Albumin binding

Using equilibrium dialysis at a fixed compound-albumin ratio, we assessed the albumin binding profiles of the tested compounds. Initially, the compounds (100 μM) in 5% bovine serum albumin-saline solution were incubated for 24 h at 25 °C. Subsequently, the solution was dialyzed in cellulose sacs with a molecular weight cutoff of 12–14 kDa (Spectra/Por, Spectrum Medical Industries Inc., CA, USA) against 25 mL of saline solution. We equilibrated the system using mechanical shaking for 72 h at 25 °C. We assessed the concentrations of the tested compounds in the starting solution and the dialyzed solution using HPLC-ES-MS/MS.



## Stability in simulated fluids and human plasma

We assessed the stability of the compounds in simulated intestinal fluid (using erythromycin as a reference compound,  $t_{1/2}$ , min = 478 min) and in human plasma (using propantheline as a reference compound,  $t_{1/2}$ , min = 2.3 min) according to our established experimental protocols.<sup>58</sup>

## Conflicts of interest

There are no conflicts to declare.

## Notes and references

- 1 A. M. Jetten, Y. Takeda, A. Slominski and H. S. Kang, Retinoic acid-related Orphan Receptor  $\gamma$  (ROR $\gamma$ ): connecting sterol metabolism to regulation of the immune system and autoimmune disease, *Curr. Opin. Toxicol.*, 2018, **8**, 66–80.
- 2 G. Eberl, ROR $\gamma$ t, a multitask nuclear receptor at mucosal surfaces, *Mucosal Immunol.*, 2017, **10**, 27–34.
- 3 I. I. Ivanov, B. S. McKenzie, L. Zhou, C. E. Tadokoro, A. Lepelley, J. J. Lafaille, D. J. Cua and D. R. Littman, The orphan nuclear receptor RORgammat directs the differentiation program of proinflammatory IL-17+ T helper cells, *Cell*, 2006, **126**, 1121–1133.
- 4 N. Manel, D. Unutmaz and D. R. Littman, The differentiation of human T(H)-17 cells requires transforming growth factor-beta and induction of the nuclear receptor RORgammat, *Nat. Immunol.*, 2008, **9**, 641–649.
- 5 X. O. Yang, B. P. Pappu, R. Nurieva, A. Akimzhanov, H. S. Kang, Y. Chung, L. Ma, B. Shah, A. D. Panopoulos, K. S. Schluns, S. S. Watowich, Q. Tian, A. M. Jetten and C. Dong, T helper 17 lineage differentiation is programmed by orphan nuclear receptors ROR alpha and ROR gamma, *Immunity*, 2008, **28**, 29–39.
- 6 T. Y. Park, S. D. Park, J. Y. Cho, J. S. Moon, N. Y. Kim, K. Park, R. H. Seong, S. W. Lee, T. Morio, A. L. Bothwell and S. K. Lee, ROR $\gamma$ t-specific transcriptional interatomic inhibition suppresses autoimmunity associated with TH17 cells, *Proc. Natl. Acad. Sci. U. S. A.*, 2014, **111**, 18673–18678.
- 7 J. F. Zambrano-Zaragoza, E. J. Romo-Martínez, J. Durán-Avelar Mde, N. García-Magallanes and N. Vibanco-Pérez, Th17 cells in autoimmune and infectious diseases, *Int. J. Inflammation*, 2014, **2014**, 651503.
- 8 M. Mosca, J. Hong, E. Hadeler, M. Hakimi, W. Liao and T. Bhutani, The Role of IL-17 Cytokines in Psoriasis, *ImmunoTargets Ther.*, 2021, **10**, 409–418.
- 9 T. Moser, K. Akgün, U. Proschmann, J. Sellner and T. Ziemssen, The role of TH17 cells in multiple sclerosis: Therapeutic implications, *Autoimmun. Rev.*, 2020, **19**, 102647.
- 10 L. Chen, G. Ruan, Y. Cheng, A. Yi, D. Chen and Y. Wei, The role of Th17 cells in inflammatory bowel disease and the research progress, *Front. Immunol.*, 2023, **13**, 1055914.
- 11 J. Zhao, Q. Lu, Y. Liu, Z. Shi, L. Hu, Z. Zeng, Y. Tu, Z. Xiao and Q. Xu, Th17 Cells in Inflammatory Bowel Disease: Cytokines, Plasticity, and Therapies, *J. Immunol. Res.*, 2021, **2021**, 8816041.
- 12 J. Gálvez, Role of Th17 Cells in the Pathogenesis of Human IBD, *ISRN Inflammation*, 2014, **2014**, 928461.
- 13 J. G. Krueger, K. A. Wharton, T. Schlitt, M. Suprun, R. I. Torene, X. Jiang, C. Q. Wang, J. Fuentes-Duculan, N. Hartmann, T. Peters, I. Koroleva, R. Hillenbrand, M. Letzkus, X. Yu, Y. Li, A. Glueck, A. Hasselberg, B. Flannery, M. Suárez-Fariñas and W. Hueber, IL-17A inhibition by secukinumab induces early clinical, histopathologic, and molecular resolution of psoriasis, *J. Allergy Clin. Immunol.*, 2019, **144**, 750–763.
- 14 J. Frieder, D. Kivelevitch and A. Menter, Secukinumab: a review of the anti-IL-17A biologic for the treatment of psoriasis, *Ther. Adv. Chronic Dis.*, 2018, **9**, 5–21.
- 15 S. Darabian, M. Badii, J. P. Dutz and J. Chan, A Retrospective Study on the Effectiveness of Ixekizumab After Treatment With Secukinumab for Patients With Active Psoriatic Arthritis, *J. Psoriasis Psoriatic Arthritis*, 2021, **7**, 13–16.
- 16 C. Paul, Ixekizumab or secukinumab in psoriasis: what difference does it make?, *Br. J. Dermatol.*, 2018, **178**, 1003–1005.
- 17 J. F. Schwensen, A. Clemmensen, C. Sand, R. Gniadecki, L. Skov, C. Zachariae, L. Iversen, M. Rasmussen and S. F. Thomsen, Effectiveness and safety of secukinumab in 69 patients with moderate to severe plaque psoriasis: a retrospective multicenter study, *Dermatol. Ther.*, 2017, **30**, e12550.
- 18 J. Berman, V. Furer, M. Berman, O. Isakov, D. Zisman, A. Haddad and O. Elkayam, Treatment with ixekizumab following secukinumab failure in patients with psoriatic arthritis: real-life experience from a resistant population, *Biologics*, 2021, **15**, 463–470.
- 19 C. Cariti, P. Dapavo, L. Mastorino, M. Ortoncelli, N. Siliquini, M. Merli, G. Avallone, S. Giordano, R. Fabrizio, S. Susca, A. Verrone, E. Stroppiana, P. Quaglino and S. Ribero, Comparison of Secukinumab and Ixekizumab in psoriasis: a real-life cohort study on the efficacy and drug survival of 445 patients, *J. Eur. Acad. Dermatol. Venereol.*, 2022, **36**, e233–e235.
- 20 Y. Y. M. Huang, J. S. Ruth and S. Hsu, Loss of efficacy of secukinumab for psoriasis at 24 to 32 weeks, *J. Am. Acad. Dermatol.*, 2016, **75**, e169.
- 21 A. Fouda, S. Negi, O. Zaremba, R. S. Gaidar, Y. S. Moroz, E. Rusanov, S. Paraskevas and J. Tchervenkov, Discovery, Synthesis, and In Vitro Characterization of 2,3 Derivatives of 4,5,6,7-Tetrahydro-Benzothiophene as Potent Modulators of Retinoic Acid Receptor-Related Orphan Receptor  $\gamma$ t, *J. Med. Chem.*, 2023, **66**, 7355–7373.
- 22 F. A. Meijer, G. J. M. Oerlemans and L. Brunsved, Orthosteric and Allosteric Dual Targeting of the Nuclear Receptor ROR $\gamma$ t with a Bitopic Ligand, *ACS Chem. Biol.*, 2021, **16**, 510–519.
- 23 F. A. Meijer, R. G. Doveston, R. M. de Vries, G. M. Vos, A. A. Vos, S. Leysen, M. Scheepstra, C. Ottmann, L. G. Milroy and L. Brunsved, Ligand-Based Design of Allosteric Retinoic Acid Receptor-Related Orphan Receptor



$\gamma$ t (ROR $\gamma$ t) Inverse Agonists, *J. Med. Chem.*, 2020, **63**, 241–259.

24 B. P. Fauber and S. Magnuson, Modulators of the nuclear receptor retinoic acid receptor-related orphan receptor- $\gamma$  (ROR $\gamma$  or ROR $\alpha$ ), *J. Med. Chem.*, 2014, **57**, 5871–5892.

25 S. M. Bronner, J. R. Zbieg and J. J. Crawford, ROR $\gamma$  antagonists and inverse agonists: a patent review, *Expert Opin. Ther. Pat.*, 2017, **27**, 101–112.

26 P. Cyr, S. M. Bronner and J. J. Crawford, Recent progress on nuclear receptor ROR $\gamma$  modulators, *Bioorg. Med. Chem. Lett.*, 2016, **26**, 4387–4393.

27 J. R. Huh, E. E. Englund, H. Wang, R. Huang, P. Huang, F. Rastinejad, J. Inglese, C. P. Austin, R. L. Johnson, W. Huang and D. R. Littman, Identification of Potent and Selective Diphenylpropanamide ROR $\gamma$  Inhibitors, *ACS Med. Chem. Lett.*, 2013, **4**, 79–84.

28 M. Kotoku, T. Maeba, S. Fujioka, M. Yokota, N. Seki, K. Ito, Y. Suwa, T. Ikenogami, K. Hirata, Y. Hase, Y. Katsuda, N. Miyagawa, K. Arita, K. Asahina, M. Noguchi, A. Nomura, S. Doi, T. Adachi, P. Crowe, H. Tao, S. Thacher, H. Hashimoto, T. Suzuki and M. Shiozaki, Discovery of Second Generation ROR $\gamma$  Inhibitors Composed of an Azole Scaffold, *J. Med. Chem.*, 2019, **62**, 2837–2842.

29 J. J. Duan, Z. Lu, B. Jiang, S. Stachura, C. A. Weigelt, J. S. Sack, J. Khan, M. Ruzanov, M. A. Galella, D. R. Wu, M. Yarde, D. R. Shen, D. J. Shuster, V. Borowski, J. H. Xie, L. Zhang, S. Vanteru, A. K. Gupta, A. Mathur, Q. Zhao, W. Foster, L. M. Salter-Cid, P. H. Carter and T. G. Dhar, Structure-based Discovery of Phenyl (3-Phenylpyrrolidin-3-yl)sulfones as Selective, Orally Active ROR $\gamma$ t Inverse Agonists, *ACS Med. Chem. Lett.*, 2019, **10**, 367–373.

30 V. B. Pandya, S. Kumar, Sachchidanand, R. Sharma and R. C. Desai, Combating Autoimmune Diseases With Retinoic Acid Receptor-Related Orphan Receptor- $\gamma$  (ROR $\gamma$  or ROR $\alpha$ ) Inhibitors: Hits and Misses, *J. Med. Chem.*, 2018, **61**, 10976–10995.

31 J. K. Barbay, M. D. Cummings, M. Abad, G. Castro, K. D. Kreutter, D. A. Kummer, U. Maharoof, C. Milligan, R. Nishimura, J. Pierce, C. Schalk-Hihi, J. Spurlino, V. M. Tanis, M. Urbanski, H. Venkatesan, A. Wang, C. Woods, R. Wolin, X. Xue, J. P. Edwards, A. M. Fourie and K. Leonard, 6-Substituted quinolines as ROR $\gamma$ t inverse agonists, *Bioorg. Med. Chem. Lett.*, 2017, **27**, 5277–5283.

32 C. Imura, A. Ueyama, Y. Sasaki, M. Shimizu, Y. Furue, N. Tai, K. Tsuji, K. Katayama, T. Okuno, M. Shichijo, K. Yasui and M. Yamamoto, A novel ROR $\gamma$ t inhibitor is a potential therapeutic agent for the topical treatment of psoriasis with low risk of thymic aberrations, *J. Dermatol. Sci.*, 2019, **93**, 176–185.

33 J. Tian, N. Sun, M. Yu, X. Gu, Q. Xie, L. Shao, J. Liu, L. Liu and Y. Wang, Discovery of N-indanyl benzamides as potent ROR $\gamma$ t inverse agonists, *Eur. J. Med. Chem.*, 2019, **167**, 37–48.

34 C. Gege, Retinoic acid-related orphan receptor gamma t (ROR $\gamma$ t) inverse agonists/antagonists for the treatment of inflammatory diseases - where are we presently?, *Expert Opin. Drug Discovery*, 2021, **16**, 1517–1535.

35 H. Gronemeyer, J. A. Gustafsson and V. Laudet, Principles for modulation of the nuclear receptor superfamily, *Nat. Rev. Drug Discovery*, 2004, **3**, 950–964.

36 X. Li, M. Anderson, D. Collin, I. Muegge, J. Wan, D. Brennan, S. Kugler, D. Terenzio, C. Kennedy, S. Lin, M. E. Labadia, B. Cook, R. Hughes and N. A. Farrow, Structural studies unravel the active conformation of apo ROR $\gamma$ t nuclear receptor and a common inverse agonism of two diverse classes of ROR $\gamma$ t inhibitors, *J. Biol. Chem.*, 2017, **292**, 11618–11630.

37 J. M. Harris, P. Lau, S. L. Chen and G. E. Muscat, Characterization of the retinoid orphan-related receptor-alpha coactivator binding interface: a structural basis for ligand-independent transcription, *Mol. Endocrinol.*, 2002, **16**, 998–1012.

38 X. Hu, Y. Wang, L. Y. Hao, X. Liu, C. A. Lesch, B. M. Sanchez, J. M. Wendling, R. W. Morgan, T. D. Aicher, L. L. Carter, P. L. Toogood and G. D. Glick, Sterol metabolism controls T(H)17 differentiation by generating endogenous ROR $\gamma$  agonists, *Nat. Chem. Biol.*, 2015, **11**, 141–147.

39 J. R. Huh, M. W. Leung, P. Huang, D. A. Ryan, M. R. Krout, R. R. Malapaka, J. Chow, N. Manel, M. Ciofani, S. V. Kim, A. Cuesta, F. R. Santori, J. J. Lafaille, H. E. Xu, D. Y. Gin, F. Rastinejad and D. R. Littman, Digoxin and its derivatives suppress TH17 cell differentiation by antagonizing ROR $\gamma$ t activity, *Nature*, 2011, **472**, 486–490.

40 N. Kumar, L. A. Solt, J. J. Conkright, Y. Wang, M. A. Istrate, S. A. Busby, R. D. Garcia-Ordonez, T. P. Burris and P. R. Griffin, The benzenesulfoamide T0901317 [N-(2,2,2-trifluoroethyl)-N-[4-[2,2,2-trifluoro-1-hydroxy-1-(trifluoromethyl)ethyl]phenyl]-benzenesulfonamide] is a novel retinoic acid receptor-related orphan receptor-alpha/gamma inverse agonist, *Mol. Pharmacol.*, 2010, **77**, 228–236.

41 M. Scheepstra, S. Leysen, G. C. van Almen, J. R. Miller, J. Piesvaux, V. Kutilek, H. van Eenennaam, H. Zhang, K. Barr, S. Nagpal, S. M. Soisson, M. Kornienko, K. Wiley, N. Elsen, S. Sharma, C. C. Correll, B. W. Trotter, M. van der Stelt, A. Oubrie, C. Ottmann, G. Parthasarathy and L. Brunsveld, Identification of an allosteric binding site for ROR $\gamma$ t inhibition, *Nat. Commun.*, 2015, **6**, 8833.

42 G. Ouvry, C. Bouix-Peter, F. Ciesielski, L. Chantalat, O. Christin, C. Comino, D. Duvert, C. Feret, C. S. Harris, L. Lamy, A. P. Luzy, B. Musicki, D. Orfila, J. Pascau, V. Pernet, A. Perrin, R. Pierre, G. Polge, C. Raffin, Y. Rival, N. Taquet, E. Thoreau and L. F. Hennequin, Discovery of phenoxyindazoles and phenylthioindazoles as ROR $\gamma$  inverse agonists, *Bioorg. Med. Chem. Lett.*, 2016, **26**, 5802–5808.

43 F. A. Meijer, I. A. Leijten-van de Gevel, R. M. de Vries and L. Brunsveld, Allosteric small molecule modulators of nuclear receptors, *Mol. Cell. Endocrinol.*, 2019, **485**, 20–34.

44 M. L. Chen, K. Takeda and M. S. Sundrud, Emerging roles of bile acids in mucosal immunity and inflammation, *Mucosal Immunol.*, 2019, **12**, 851–861.

45 S. Hang, D. Paik, L. Yao, E. Kim, J. Trinath, J. Lu, S. Ha, B. N. Nelson, S. P. Kelly, L. Wu, Y. Zheng, R. S. Longman,



F. Rastinejad, A. S. Devlin, M. R. Krout, M. A. Fischbach, D. R. Littman and J. R. Huh, Bile acid metabolites control TH17 and Treg cell differentiation, *Nature*, 2019, **576**, 143–148.

46 D. Paik, L. Yao, Y. Zhang, S. Bae, G. D. D'Agostino, M. Zhang, E. Kim, E. A. Franzosa, J. Avila-Pacheco, J. E. Bisanz, C. K. Rakowski, H. Vlamakis, R. J. Xavier, P. J. Turnbaugh, R. S. Longman, M. R. Krout, C. B. Clish, F. Rastinejad, C. Huttenhower, J. R. Huh and A. S. Devlin, Human gut bacteria produce TH17-modulating bile acid metabolites, *Nature*, 2022, **603**, 907–912.

47 R. A. Quinn, A. V. Melnik, A. Vrbanac, T. Fu, K. A. Patras, M. P. Christy, Z. Bodai, P. Belda-Ferre, A. Tripathi, L. K. Chung, M. Downes, R. D. Welch, M. Quinn, G. Humphrey, M. Panitchpakdi, K. C. Weldon, A. Aksенов, R. da Silva, J. Avila-Pacheco, C. Clish, S. Bae, H. Mallick, E. A. Franzosa, J. Lloyd-Price, R. Bussell, T. Thron, A. T. Nelson, M. Wang, E. Leszczynski, F. Vargas, J. Gauglitz, M. Meehan, E. Gentry, T. Arthur, A. Komor, O. Poulsen, B. Boland, J. Chang, W. Sandborn, M. Lim, N. Garg, J. Lumeng, R. Xavier, B. Kazmierczak, R. Jain, M. Egan, K. Rhee, D. Ferguson, M. Raffatellu, H. Vlamakis, G. Haddad, D. Siegel, C. Huttenhower, S. Mazmanian, R. Evans, V. Nizet, R. Knight and P. C. Dorrestein, Global chemical effects of the microbiome include new bile-acid conjugations, *Nature*, 2020, **579**, 123–129.

48 S. Brogi, M. Brindisi, S. Butini, G. U. Kshirsagar, S. Maramai, G. Chemi, S. Gemma, G. Campiani, E. Novellino, P. Fiorenzani, J. Pinassi, A. M. Aloisi, M. Gynther, R. Venskutonyté, L. Han, K. Frydenvang, J. S. Kastrup and D. S. Pickering, (S)-2-Amino-3-(5-methyl-3-hydroxyisoxazol-4-yl)propanoic Acid (AMPA) and Kainate Receptor Ligands: Further Exploration of Bioisosteric Replacements and Structural and Biological Investigation, *J. Med. Chem.*, 2018, **61**, 2124–2130.

49 K. Frydenvang, D. S. Pickering, G. U. Kshirsagar, G. Chemi, S. Gemma, D. Sprogøe, A. M. Kærn, S. Brogi, G. Campiani, S. Butini and J. S. Kastrup, Ionotropic Glutamate Receptor GluA2 in Complex with Bicyclic Pyrimidinedione-Based Compounds: When Small Compound Modifications Have Distinct Effects on Binding Interactions, *ACS Chem. Neurosci.*, 2020, **11**, 1791–1800.

50 S. Liu, D. Liu, R. Shen, D. Li, Q. Hu, Y. Yan, J. Sun, F. Zhang, H. Wan, P. Dong, J. Feng, R. Zhang, J. Li, L. Zhang and W. Tao, Discovery of a novel ROR $\gamma$  antagonist with skin-restricted exposure for topical treatment of mild to moderate psoriasis, *Sci. Rep.*, 2021, **28**, 913.

51 S. Rauhamäki, P. A. Postila, S. Lätti, S. Niinivehmas, E. Multamäki, K. R. Liedl and O. T. Pentikäinen, Discovery of Retinoic Acid-Related Orphan Receptor  $\gamma$ t Inverse Agonists via Docking and Negative Image-Based Screening, *ACS Omega*, 2018, **3**, 6259–6266.

52 L. A. Solt and T. P. Burris, Action of RORs and their ligands in (patho)physiology, *Trends Endocrinol. Metab.*, 2012, **23**, 619–627.

53 W. L. Jorgensen, D. S. Maxwell and J. Tirado-Rives, Development and Testing of the OPLS All-Atom Force Field on Conformational Energetics and Properties of Organic Liquids, *J. Am. Chem. Soc.*, 1996, **118**, 11225–11236.

54 S. Fujita-Sato, S. Ito, T. Isobe, T. Ohyama, K. Wakabayashi, K. Morishita, O. Ando and F. Isono, Structural basis of digoxin that antagonizes ROR $\gamma$ t receptor activity and suppresses Th17 cell differentiation and interleukin (IL)-17 production, *J. Biol. Chem.*, 2011, **286**, 31409–31417.

55 S. Brogi, A. Fiorillo, G. Chemi, S. Butini, M. Lalle, A. Ilari, S. Gemma and G. Campiani, Structural characterization of *Giardia duodenalis* thioredoxin reductase (gTrxR) and computational analysis of its interaction with NBDHEX, *Eur. J. Med. Chem.*, 2017, **135**, 479–490.

56 B. Battah, G. Chemi, S. Butini, G. Campiani, S. Brogi, G. Delogu and S. Gemma, A Repurposing Approach for Uncovering the Anti-Tubercular Activity of FDA-Approved Drugs with Potential Multi-Targeting Profiles, *Molecules*, 2019, **24**, 4373.

57 H. Sirous, G. Chemi, S. Gemma, S. Butini, Z. Debyser, F. Christ, L. Saghaei, S. Brogi, A. Fassihi, G. Campiani and M. Brindisi, Identification of Novel 3-Hydroxy-pyran-4-One Derivatives as Potent HIV-1 Integrase Inhibitors Using in silico Structure-Based Combinatorial Library Design Approach, *Front. Chem.*, 2019, **7**, 574.

58 M. T. Gabr and S. Brogi, MicroRNA-Based Multitarget Approach for Alzheimer's Disease: Discovery of the First-In-Class Dual Inhibitor of Acetylcholinesterase and MicroRNA-15b Biogenesis, *J. Med. Chem.*, 2020, **63**, 9695–9704.

